PHYC40970: Advanced Laboratory II

# Mie Scattering

**Author:** Lainey Ward
**Student ID:** 18365881
**Supervisor:** Dr. Brian Vohnsen
March 8, 2022

## Abstract

Mie scattering is the elastic scattering of a plane wave by a homogeneous sphere. In this experiment, the angular dependence of Mie scattering is demonstrated using a red and green laser, a spectrometer and three suspensions of polystyrene latex spheres. The theoretical size parameters of the samples lie in the range $(9 \pm 2, 45 \pm 8)$. The prominence of Mie scattering features within scattered intensity distributions are found to be highly dependent on the diameter of the spheres, as well as the sample concentration. From these distributions, it is shown that the size parameter is proportional to the sphere diameter and inversely proportional to the laser wavelength. The experimental findings for the 3.0 $\mu m$ sample mostly fail to align with that predicted by Drake and Gordon, as well as the MiePython module. The fitting parameters for both functions universally underestimate the diameter of the spheres and the refractive index of the spheres relative to the surrounding medium. This equates to a mean percent difference of $-36\%$ and $-100\%$ from their respective theoretical values. Theoretical intensity distributions are also produced using MiePython, for various values of parameters $a$, $\lambda$ and $m$.

## 1 Introduction

Mie Scattering is the elastic scattering of a plane wave by a homogeneous sphere. It is often referred to as aerosol particle scattering, as it takes place with suspended particles in the lower atmosphere. It is responsible for the grey or white colour of clouds.

In this experiment, the angular dependence of Mie scattering is demonstrated for polystyrene latex spheres using a modified experimental method of Drake and Gordon (1985). Two primary Mie scattering functions obtained from Drake and Gordon (1985) and the Python module MiePython, are fit to the experimental data. It is demonstrated experimentally that Mie scattering is highly dependent on the sphere radius, and to a lesser extent, the wavelength of incident light. This is verified computationally, from which a dependence on the refractive index of the spheres with respect to its surrounding medium is also shown.

## 2 Theory

### 2.1 Mie's Theory

Gustav Mie wrote his classic paper on light scattering by small spherical particles in 1908. In this paper he proposed a method by which to compute the scattering of light off of these spheres using Maxwell's electromagnetic theory. Using this method, he explained how gold colloids change colour with changing particle diameter. [1]

Although Mie's theory is named after Gustav Mie, he was not the first to formulate his scattering solution. Therefore, Peter Debye and Ludvig Lorenz are also accredited to the development of Mie's theory. This theory commonly refers to the scattering of a plane electromagnetic wave by a homogeneous, isotropic sphere. The theory does not refer to an independent physical theory or law, but rather a collection of solutions to Maxwells equations for such scattering. [1]

Many adaptations have since been made to Mie, Debye and Lorenz's original solutions. Today, Mie's theory can be computed for coated, multilayer, distorted, magnetic and clusters of spheres. [1]

### 2.2 Mie Scattering

The degree of scattering from a sphere is often described in terms of a dimensionless, size parameter $(ka)$, as follows: [2] [3]

$$ka = \frac{2\pi}{\lambda} ma \tag{1}$$

with $m$, the refractive index of the sphere relative to the surrounding medium, $a$, the sphere diameter, and $\lambda$, the wavelength of incident light in the medium.

$m$ is a complex number, where the real and imaginary parts represent the normal refractive index and the absorption coefficient of the sphere. For the purpose of simplicity, it is assumed that the spheres used throughout the experiment are non-absorbing and therefore have a zero imaginary part.

It is apparent from Eq. 1 that the size parameter is proportional to $m$ and $a$, and inversely proportional to $\lambda$. The relations for $a$ and $\lambda$ are demonstrated experimentally.

### 2.3 Drake and Gordon Approximation

Drake and Gordon use an adapted Rayleigh-Debye approximation to model Mie scattering. Their findings indicate that this model fits to the experimental data relatively well. Weiner, Rust and Donnelly also use their own corrected, however unlisted, version of Drake and Gordon's formula, to an even greater degree of success. [3]

The experimental set-up described in Section 3 is similar in nature to that of Drake and Gordon. Therefore, it is anticipated that this model will also fit to the obtained data well.

The model determines the intensity of the scattered radiation with respect to the scattered angle. To correct for the refraction at the air-glass-water interfaces and foreshortening, the actual scattering angle ($\theta$) is determined from the observed scattering angle as follows:

$$\theta = \sin\left(\frac{\sin\theta_o}{n}\right)^{-1} \tag{2}$$

With $n$, the index of refraction of the surrounding medium relative to air.

The model also requires parameters $ka$, $x$ and $J_1(x)$ to be first defined. $ka$ is determined from Eq. 1, and $x$ and $J_1(x)$ from the following: [2]

$$x = ka\left(1 + m^2 - 2m\cos\theta\right) \tag{3}$$

$$J_1(x) = \frac{\sin x - x\cos x}{x^2} \tag{4}$$

Once these three parameters are define, Drake and Gordon's approximation can be given by:

$$I(\theta) = I_0\left(\frac{3|J_1(x)|}{x} + x^{-3/2}\right)^2 \frac{1+\cos^2\theta}{2} \tag{5}$$

$I_0$ can be defined in terms of $ka$, the electric field and the distance from the sphere. However, this term is absorbed by a general scaling coefficient throughout the analysis.

For the values of $n$, $m$, $\lambda$ and $ka$ used by Drake and Gordon, the resulting intensity distribution should feature local maxima occurring at large $I(\theta)$ for small $\theta$, and small $I(\theta)$ for large $\theta$. The degree of scattering is proportional to the number of maxima within a given range, and therefore inversely proportional to the angular displacement between maxima. [2] It is also inversely proportional to the sphere size parameter.

### 2.4 MiePython Approximation

MiePython is a Python module that uses a method described by Wiscombe (1979) to determine the Mie scattered intensities in the planes parallel ($I_{PAR}$) and perpendicular ($I_{PERP}$) to the incident light. The module can also determine the scattered amplitudes for the spheres ($S1$ and $S2$), having units $sr^{-0.5}$. These amplitudes are related to the parallel and perpendicular intensities as follows: [4]

$$I_{\mathrm{PERP}} = |S1|^2 \tag{6}$$

$$I_{\mathrm{PAR}} = |S2|^2 \tag{7}$$

These MiePython modules are fitted to the experimental data with parameters $m$ and $x$.

### 2.5 Scattering Cross Section

Cox et al. (2002) notes that the scattering cross section for a sample is:

$$\sigma = \frac{\log_{10}(D)}{\rho L} \tag{8}$$

with $D$, the optical density of the sample, $L$, the length of the cuvette, and, $\rho$, the sample density. The sample density is unknown throughout the experiment and so $\sigma$ cannot be directly calculated. $D$ is the ratio of the light incident to the light transmitted through the sample, and is proportional to $I(\theta)$. Therefore, the common logarithm of $I(\theta)$ is proportional to the scattering cross section. [5] For this reason, the intensity distribution plots are presented with y-axes $I(\theta)$ and a $\log_{10}(I(\theta))$.

## 3 Experiment

### 3.1 Configuration

The experimental apparatus consists of a OS-8525A 650 $nm$ red and a OS-8458B 515 $nm$ green diode laser, a neutral density filter, a USB650 Red Tide spectrometer, SpectraSuite software, a Branson 200 Ultrasonic cleaner, and a cuvette of square cross section. The Red Tide is mounted on the rotating arm of a manual rotary stage. The cuvette is placed on a small platform in the centre of the stage. The neutral density filter attenuates the laser's 1 $mW$ power output, preventing easy saturation of the spectrometer.

Concentrated Sigma-Aldrich PSL solutions are used with diameters of 3.0, 1.1 and 0.8 $um$.

The optical system must be arranged methodically, before using each laser. The first and final components of the optical system, (the laser and spectrometer), are aligned with no other components in the system. The laser is directly incident on the spectrometer input, at an angle of 0°. Next, a cuvette of distilled water is placed on the stage and again, the system is adjusted to ensure the laser is still incident on the input. Finally, the neutral density filter is added.

### 3.2 Method

Following the system alignment, the sphere sample is prepared. A small drop of the sphere solution is added to a 10 $ml$ measuring cylinder of distilled water. The solution is repeatedly added until the suspension is cloudy yet transparent, so as to assume it is in the single-scattering regime. The number of spheres per volume is not listed on the sphere's specification sheets and so the quantitative concentrations of each sample are unknown.[6] [7] However, the qualitative concentrations of various samples of the same sphere diameter can be known.

To ensure optical stability, the laser is allowed to warm up for 20 minutes. The cuvette is cleaned and placed in the ultrasonic cleaner to agitate the sample. Then, the sample is placed on the rotating stage, and the offset angle, the angle at which the laser is directly incident on the spectrometer input, is measured. This value is subtracted from each angular reading, and re-measured when the system is re-aligned for the second laser.

The spectrometer graph is saved from the SpectraSuite software for angles in the range $(10 - 60)°$, in degree or half-degree increments with the first line of the Vernier scale aligned to the baseline. This process is completed in series for the distilled water, 3.0, 1.1 and 0.8 $um$ samples for both the red and green lasers. Measurements are taken rapidly to reduce the effects of sample sedimentation on the intensity output of the system, in particular for the 3.0 $um$ sample.

All spectrometer measurements are recorded in a dark room, to reduce the inference of background noise on the spectrometer signal.

**SpectraSuite Software**

The SpectraSuite software graphs the number of counts against the wavelengths of light obtained by the spectrometer. The integration time and the number of averages are set so as to ensure the number of counts maximises at $\sim 10°$. These values are found to be optimised at 20 $ms$ and 400 averages. Thus, the total time to obtain a spectrum is 8 $s$. For simplicity, both parameters are kept constant for every sample throughout the experiment. However, the analysis could be amended to account for changes in integration time, assuming the relation between integration time and the number of counts is linear.

The background signal is recorded and subtracted before measurements are taken for each sample. The spectrometer plot is examined following each measurement, and the background signal is re-recorded at the onset of baseline drift.

## 4 Results & Analysis

The analysis of experimental data is undertaken in sections, according to the diameter of the particle under consideration. The effects of sphere concentration and laser wavelength are discussed within each section, alongside an ongoing discussion about the effects of sphere diameter.

Intensity and angle readings are collected and corrected in accordance with Section 3. Data is collected for the system configured with the red laser first, followed by the green laser.

The manipulation of data, including uncertainty propagation and fit function application, is outlined in detail in the attached Jupyter notebook.

### 4.1 Determination of Intensity

The spectrometer graphs are saved as text files consisting of corresponding count and wavelength values, and are imported into Python. The uncertainty on counts and wavelengths is presumed to be negligible.

Using a non-linear least squares method, a Gaussian function is fitted to the data. This function takes the form:

$$Counts = A \exp\left[-\frac{(\lambda - \mu^2)}{2\sigma^2}\right] \tag{9}$$

with fitting parameters $A$, the height of the curve's maximum, $\mu$, the position of the maximum, and $\sigma$, the stan-

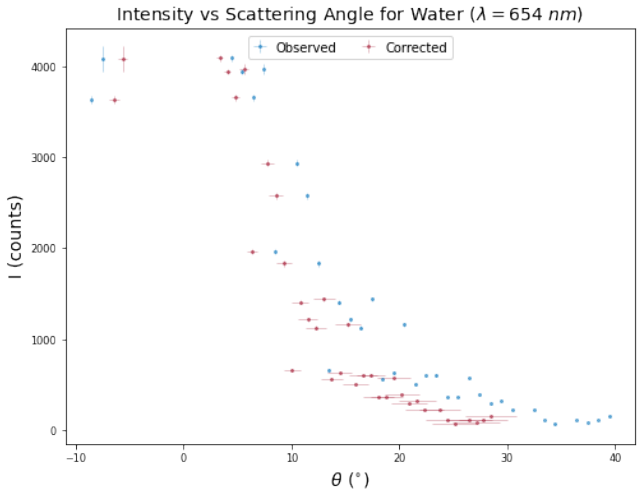


**(a)** The observed and corrected angular distribution for intensity for the water sample using the red laser.

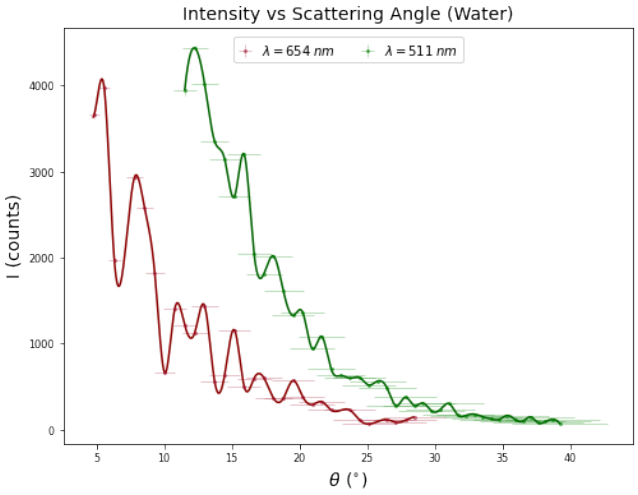


**(b)** The angular distribution of the scattered intensity for the water sample using the red and green lasers.

**Fig. 1:** Water sample.

dard deviation. To optimise the accuracy of the Gaussian, the function is only fitted to data within $\pm 15\ nm$ of the laser's wavelength. Each plot is examined visually and those that do not follow a Gaussian distribution are disregarded.

The intensity for each angle is given by the corresponding $A$ parameter. The laser wavelength for each investigation is given by the mean of the $\mu$ parameters across all angles. These wavelengths are given in Table 1, alongside a list of the laser-sample combinations analysed in the following sections. The mean wavelength of the red laser is found to be $(653.7 \pm 0.3)\ nm$, greater than its expected value of $650\ nm$. Similarly, the mean wavelength of the green laser is $(511.1 \pm 0.5)\ nm$, lower than its expected value of $515\ nm$.

| Laser | $a$ $(\mu m)$ | Concentration | $\lambda_{exp}$ $(nm)$ |
|---|---|---|---|
| Red | - | - | $653.9 \pm 0.1$ |
| Red | 3.0 | Low | $653.4 \pm 0.8$ |
| Red | 3.0 | High | $653.9 \pm 0.7$ |
| Red | 1.1 | Low | $653.8 \pm 0.7$ |
| Red | 1.1 | High | $653.3 \pm 0.9$ |
| Red | 0.8 | High | $653.9 \pm 0.7$ |
| Green | 3.0 | High | $510.9 \pm 0.5$ |
| Green | - | - | $511.3 \pm 0.8$ |

**Table 1:** The mean $\lambda$ parameters determined by the Gaussian fits for the experimental combinations of laser wavelength, sphere diameter and concentration.

## 4.2 Water

As discussed in Section 2.3, the observed angle is corrected using Eq. 2. The angular distribution of the scattered intensity is shown in Fig. 1a, for both the observed angle and corrected angle. The conversion reduces the angular range and is symmetric about the transmission angle. Despite the very low observed angular uncertainty, the conversion introduces a significant uncertainty into the corrected angle. This uncertainty is increasingly pronounced at higher angles.

The angular distribution of the scattered intensity from the distilled water sample is plotted in Fig. 1b for both the red and green laser. For the purpose of visualisation, a smoothing spline is fit to both sets of data.

The scattered intensity for the green laser is consistently higher than that of the red laser, at a given angle. This may be attributed to a systematic difference introduced following the re-configuration of the optical system for the green laser.

Both distributions follow an exponential curve overlaid by apparent local maxima and minima. In the range $(15° \leq \theta \leq 25°)$, these maxima and minima occur at approximately the same angles for both distributions.

As the water is distilled, it is presumed that there are negligible scatterers with diameter of the order $\mu m$ present in the sample. Thus, the presence of Mie scattering should not be evident. Rather, these local maxima

and minima are most likely noise. A greater angular resolution is necessary to confirm this assumption.

### 4.3 $a = 3\ \mu m$

The angular distribution of the scattered intensity for the 3.0 $\mu m$ sample is obtained for the red and green laser, with the former at both a 'low' and 'high' concentration.

The distribution for the low concentration is shown in Fig. 2, with a broad angular range of $(-43, 43)°$. It is worth noting that the scattering in Fig. 2 appears to be symmetric about the transmission angle, 0°.

The features of the plot align more closely with that of the water sample in Fig. 1b, as opposed to that noted by Drake and Gordon, under similar conditions. This implies that the density of scatters is too low to produce a discernible Mie scattering effect, and so the concentration of spheres is increased.

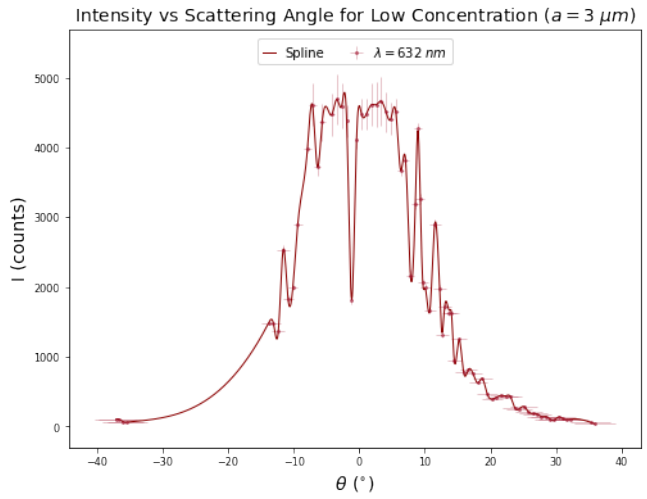


**Fig. 2:** The angular distribution of intensity for the low concentration 3 $\mu m$ sample using the red laser. Note the symmetry about the transmission angle.

The same high concentration sample is used for both the red and green laser. The angular distribution of the scattered intensity for this sample is shown in Fig. 3a. This plot is also shown for the common logarithm of intensity in Fig. 3b. Again, a smoothing spline has been fit to the data in both plots.

Periodic local maxima are apparent in both figures, particularly in Fig. 3b. These maxima are indicative of the Mie scattering effect. The local knee points of both figures, as well as the angular displacement between adjacent knees, are given in Table 2 and 3. In the common logarithm plot, the mean angular displacement is 7.4° and 8.6° for the red and green laser respectively.

| $\lambda$ $(nm)$ | $k_1$ (°) | $k_2$ (°) | $k_3$ (°) | $\Delta k_{21}$ (°) | $\Delta k_{32}$ (°) |
|---|---|---|---|---|---|
| 654 | 12.84 | 21.83 | 31.36 | 8.99 | 9.40 |
| 511 | 15.65 | 23.23 | 31.15 | 7.58 | 7.92 |

**Table 2:** Angular position of knees and the displacement between adjacent knees corresponding to each laser plot in Fig. 3a.

| $\lambda$ $(nm)$ | $k_1$ (°) | $k_2$ (°) | $k_3$ (°) | $k_4$ (°) | $\Delta k_{21}$ (°) | $\Delta k_{32}$ (°) | $\Delta k_{43}$ (°) |
|---|---|---|---|---|---|---|---|
| 654 | 14.11 | 22.26 | 31.36 | - | 8.15 | 9.10 | - |
| 511 | 16.40 | 23.36 | 31.52 | 38.59 | 6.96 | 8.16 | 7.07 |

**Table 3:** Angular position of knees and the displacement between adjacent knees corresponding to each laser plot in Fig. 3b.

As discussed in Section 2, Drake and Gordon note that the angular displacement is proportional to the sample's size parameter. This implies that sample has a greater size parameter for the green laser, than for the red laser. This is in accordance with the theoretical size parameters calculated using Eq. 14, listed in Table 4.

| $\lambda$ $(nm)$ | $a$ $(\mu m)$ | $ka$ |
|---|---|---|
| $653.7 \pm 0.3$ | $3.0 \pm 0.3$ | $35 \pm 6$ |
| $511.1 \pm 0.5$ | $3.0 \pm 0.3$ | $45 \pm 8$ |
| $653.7 \pm 0.3$ | $1.1 \pm 0.1$ | $13 \pm 2$ |
| $653.7 \pm 0.3$ | $0.80 \pm 0.08$ | $9 \pm 2$ |

**Table 4:** $\lambda$ and $a$ combinations substituted into Eq. 1, and the corresponding system size parameter. $m$ is assumed constant, and calculated as $1.2 \pm 0.1$.

The difference between the mean angular displacement for the red and green laser is relatively small at $\sim 1.2°$. This small disparity can be attributed to the similarity of the laser wavelengths (511 and 654 $nm$). Therefore, a laser of a dissimilar wavelength to that of the red and green would make the inverse relationship between size angular displacement and wavelength much more visually evident.

#### Drake and Gordon Fit

Using an ODR model, Eq. 5 is fitted to the data in both figures in Fig. 3. For Fig. 3a this function takes the form:

$$I(\theta) = C\left(\frac{3|J_1|}{x} + x^{-3/2}\right)^2 \frac{1}{2}\left(1 + \cos^2(\theta)\right) + D \quad (10)$$

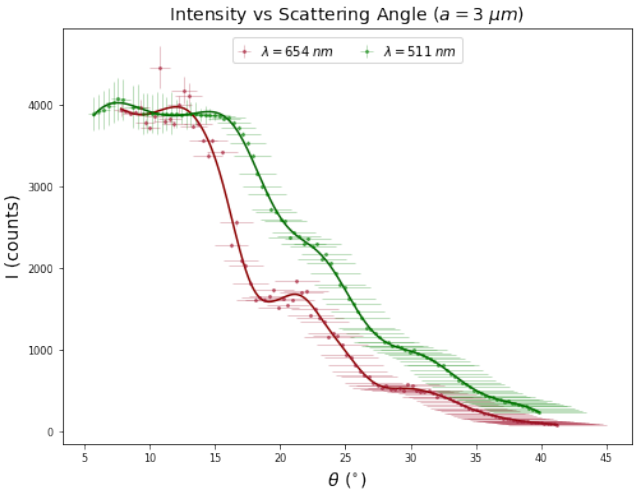


**(a)** The angular distribution of intensity for the 3 $\mu m$ sample using the red and green lasers.

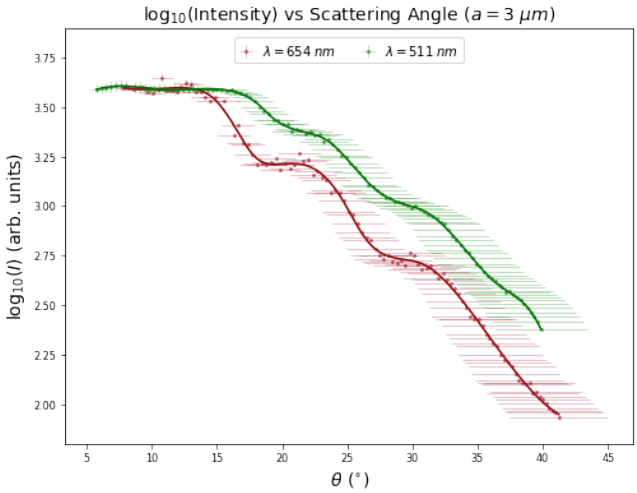


**(b)** Fig. 3a displayed with a common logarithm intensity axis.

**Fig. 3:** 3 $\mu m$ sample.

Similarly for Fig. 3b, this function is:

$$\log_{10}\left(I(\theta)\right) = C\log_{10}\left[\left(\frac{3|J_1|}{x} + x^{-3/2}\right)^2 \frac{1}{2}\left(1+\cos^2(\theta)\right)\right] + D \tag{11}$$

By fixing the value of $\lambda$, $m$, $a$, $C$ and $D$ are the only required fitting parameters. $C$ and $D$ function only as scaling parameters.

The resulting fits are shown in Fig. 4. It is apparent in both figures that the Drake and Gordon approximation (black) provides a poor fit to the data. In response, the function is fit to various subsets of the data, and the closest fits are shown (blue). Within the restricted range, the fitting functions provide a much better fit to the data. The fitting parameters for all four fits are given in Table 5.

By examining the $m$ and $a$ parameters, especially those of the subset fits, it is apparent that they are significantly lower than their expected values of $\sim 2.2$ and 3.0 $\mu m$, respectively. The mean values of these parameters, calculated from the subset fits only, are $(1.10 \pm 0.04)$ and $(2.2 \pm 0.2)$ $\mu m$. This equates to a percent difference of $-100$

By fixing the values of $m$ and $n$ to $(1.10 \pm 0.04)$ and $(1.2 \pm 0.1)$, the refractive index of the spheres with respect to air is calculated to be $(1.3 \pm 1.1$. This is also significantly lower than its expected value of $\sim 1.66$.

Furthermore, the undersized $a$ parameter indicates that the spheres have undergone shrinkage from their original manufactured size. This is plausible given the long period that they have been retained in the laboratory.

| Fig. | Data | $m$ | $a$ ($\mu m$) | $C$ | $D$ ($counts$) |
|---|---|---|---|---|---|
| 3a | All | $1.18 \pm 0.03$ | $1.7 \pm 0.1$ | $(3.1 \pm 0.1)10^5$ | $18 \pm 27$ |
| 3a | Subset | $1.08 \pm 0.08$ | $2.2 \pm 0.4$ | $(1.3 \pm 0.2)10^5$ | $986 \pm 90$ |
| 3b | All | $1.12 \pm 0.03$ | $2.1 \pm 0.1$ | $(8.2 \pm 0.3)10^{-1}$ | $5.08 \pm 0.07$ |
| 3b | Subset | $1.11 \pm 0.01$ | $2.1 \pm 0.1$ | $(5.1 \pm 0.2)10^{-1}$ | $4.44 \pm 0.04$ |

**Table 5:** ODR parameters corresponding to the Drake and Gordon approximation fits in Fig. 4.

The analysis of fitting parameters has been limited to the red laser only and the Drake and Gordon approximation provides a very poor fit to the scattered intensity distribution of the green laser.

### MiePython Fit

Using an ODR model, the MiePython parallel and perpendicular scattered intensity modules are fitted to the red laser intensity distribution in Fig. 5a. The perpendicular fit is comparable to that of Drake and Gordon fit in Fig. 4a.

As discussed in Section 2, the perpendicular and parallel scattered intensities are composed of amplitudes $S1$ and $S2$. Therefore, the MiePython $S1$ and $S2$ modules are also fit to the data, as shown in Fig. 5b. The $S2$ function provides a reasonable fit to the data, particularly at low scattering angles. The fitting parameters for both functions are given in Table 6. Once again it is apparent that parameters $m$ and $a$ are undersized with

respect to their expected values. However, $m$ and $a$ lie within and just outside the uncertainty range of those determined from the Drake and Gordon function.

Once again, the parallel, perpendicular, $S1$ and $S2$ modules provide a very poor fit to the scattered intensity distribution of the green laser.

| Plot | $m$ | $a$ ($\mu m$) | $C$ ($10^3$) | $D$ ($10^2$ $counts$) |
|---|---|---|---|---|
| S1 | $1.117 \pm 0.003$ | $2.05 \pm 0.02$ | $3.9 \pm 0.1$ | $-4.1 \pm 0.7$ |
| $S2$ | $1.123 \pm 0.002$ | $2.01 \pm 0.02$ | $3.9 \pm 0.1$ | $-5.2 \pm 0.4$ |

**Table 6:** ODR parameters corresponding to the MiePython fits in Fig. 5.

### 4.4 $a = 1.1\ \mu m$

The angular distribution of the scattered intensity for the 1.1 $\mu m$ sample is obtained for the red laser, at both a low and high concentration. These distributions are shown in Fig. 6a, alongside their common logarithm in Fig. 6b.

As in tSection 4.2, the low concentration distribution is more comparable to that of the water sample, than that expected from Mie scattering.

For the high concentration sample, there appear to be no distinct local maxima or minima in either figures, as in the case of the 3.0 $\mu m$ sample. According to Table 4, the size parameter of the sample is $\sim 13$ and so the angular displacement between maxima is most likely greater than the angular range under consideration. Therefore, the effects of Mie scattering are not initially apparent in the figure. In Fig. 6b, the data appears to form a portion of a single local maximum, as opposed to three distinct maxima in the case of the 3 $\mu m$ sample.

### 4.5 $a = 0.8\ \mu m$

The angular distribution of the scattered intensity for the 0.8 $\mu m$ sample is shown for the red laser in Fig. 7. Again, the angular displacement between maxima is too great to distinguish distinctive features of Mie scattering.

### 4.6 MiePython

Thus far the experimental analysis is limited by the availability of laser of varying wavelengths, spheres of varying radii and spheres of varying refractive indices. The MiePython module can be implemented to gain a more thorough understanding into the effects of these variables on Mie scattering.

Theoretical angular distributions for scattered intensities are produced using the MiePython module for unpolarised scattered intensities in Fig. 8. These are computed for three values of each variable; $a$, $\lambda$ and $m$. Each set of values are the first, second and third multiple of the lowest value.

In Fig. 8a, there is a singular $a = 1\ \mu m$ local maximum in the range $(17° \leq \theta \leq 34°)$. This maximum encompasses approximately three local maxima of the $a = 3\ \mu m$ plot and nine local maxima of the $a = 9\ \mu m$ plot. Thus it can be concluded that the angular displacement between maxima is inversely proportional to the value of $a$.

Furthermore, it is apparent that at low angles, higher intensities are attained for lower values of $a$.

In Fig. 8b, the angular displacement between maxima is proportional to $\lambda$. The local maximum of $\lambda = 900\ nm$ in the range $(18° \leq \theta \leq 27°)$ encompasses approximately two wavelengths of the $\lambda = 600\ nm$ plot and three wavelengths of the $\lambda = 300\ nm$ plots. This is in accordance with the experimental findings in Section X, in which the red laser system has a smaller angular displacement than that if the green system.

Finally, in Fig. 8c, the wavelengths are more distorted and less sinusoidal in nature than those of Fig. 8a and 8b. Regardless, the angular displacement between maxima is inversely proportional to the value of $m$. The singular local maximum encompasses three and six wavelengths of the $m = 1.45$ and $m = 2.7$ plots.

This understanding of the theoretical relationships between the discernibility of Mie scattering features and variables $a$, $\lambda$ and $m$ can be used to guide and improve the experimental method and configuration. For example, using the same red laser from the experiment, it is more advantageous to use spheres with diameters in the range $(3, 9)\ \mu m$, than that used in Sections 4.2-4.5 $(0.8 - 3)\ \mu m$.

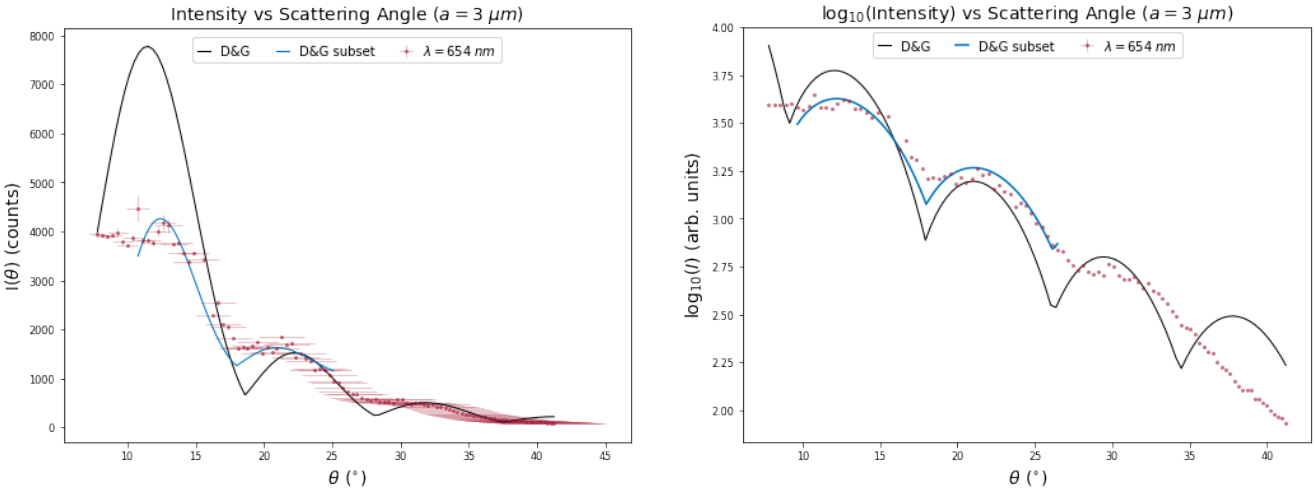


**(a)** **(b)**

**Fig. 4:** Fig. 3a and 3b fitted to the Drake and Gordon approximation, for the red laser only. Two selected subsets of the data have also been fitted.

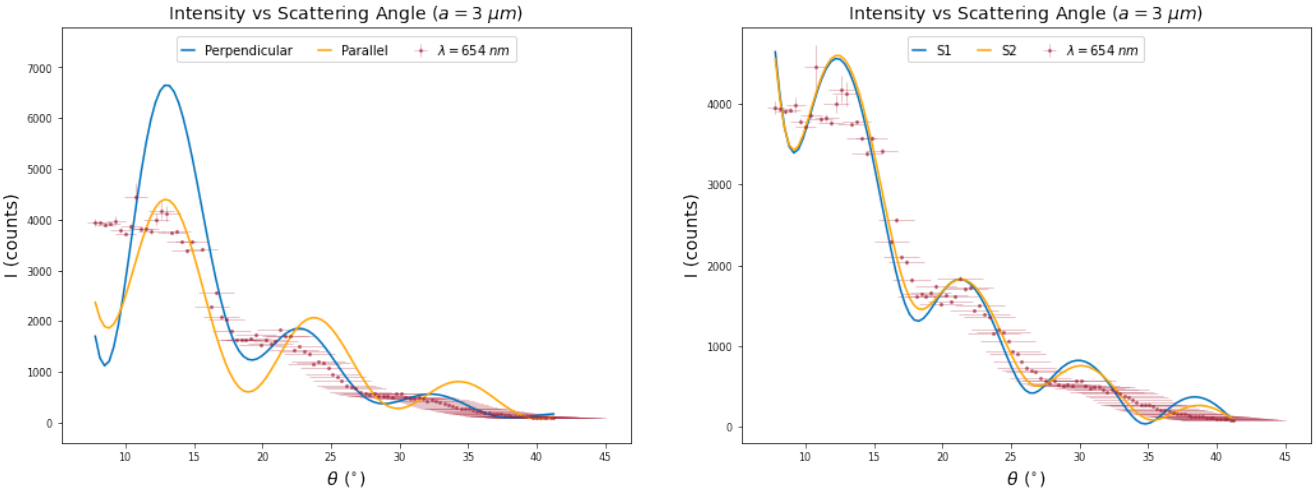


**(a)** **(b)**

**Fig. 5:** Fig. 3a and 3b fitted to the MiePython intensity and intensity amplitude modules, for the red laser only. Two selected subsets of the data have also been fitted.

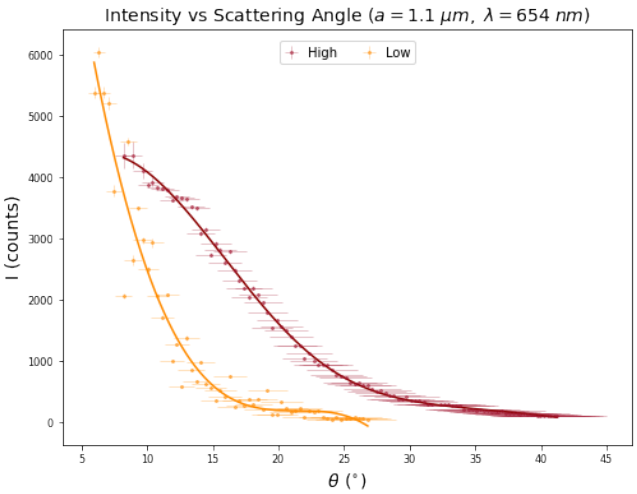


**(a)** The angular distribution of intensity for the 1.1 $\mu m$ sample at a low and high concentration, using the red laser.

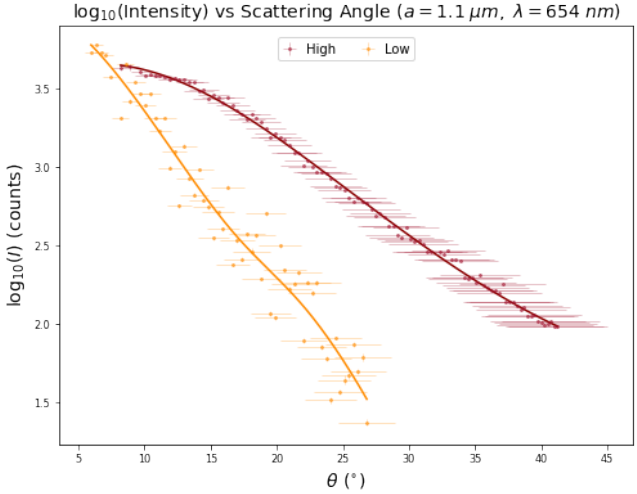


**(b)** Fig. 6a displayed with a common logarithm intensity axis.

**Fig. 6:** 1.1 $\mu m$ sample.

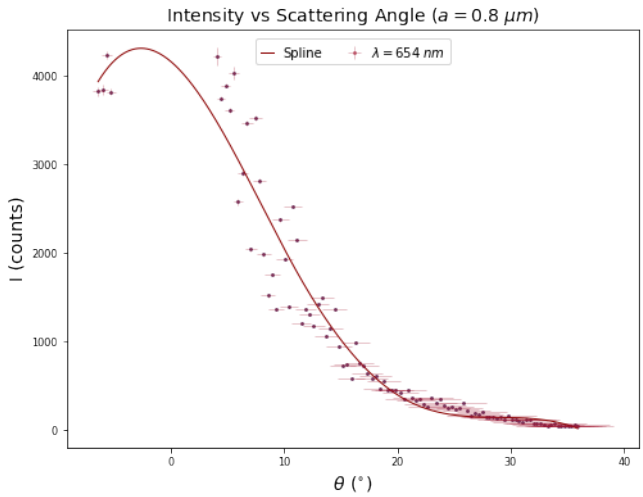


**Fig. 7:** The angular distribution of intensity for the 0.8 $\mu m$ sample using the red laser.

## 5 Conclusion

In this experiment, Mie scattering is demonstrated using a red and green laser, three scattering samples of varying diameter and a spectrometer. For various combinations of laser and scattering samples, a plot of the angular distribution of scattered light intensity is produced. The prominence of Mie scattering features within these plots is found to be highly dependent on the diameter of the polystyrene latex spheres, as well as the sample concentration.

The theoretical size parameters of the experimental data are found to lie in the range $(9 \pm 2, 45 \pm 8)$. Using the angular displacement between adjacent knee points, it is shown that wavelength and the size parameter are inversely proportional, and sphere diameter and the size parameter are proportional. This is in accordance with theory, as discussed by Drake and Gordon (1985).

The 1.1 and 0.8 $\mu m$ samples provide little insight into the features of Mie scattering, as the angular displacement between maxima for these samples is greater than the angular range under consideration.

The experimental findings for the 3.0 $\mu m$ sample mostly fail to align with that predicted by Drake and Gordon, as well as the MiePython module. A moderate fit is obtained for the former using only for a small subset of the data. The latter provides a good fit at low angles using the $S2$ scattering amplitude module. The fitting parameters universally underestimate the values of $a$ and $m$. This may indicate that the diameter of the spheres has shrunk from that reported by the manufacturer.

Theoretical intensity distributions are produced using MiePython, for various values of parameters $a$, $\lambda$ and $m$. The spread of a local maximum is found to be proportional to $\lambda$ and inversely proportional to both $a$ and $m$.

Overall, the value and accuracy of the experimental findings would be significantly improved by the use of spheres with diameters in the range $(3, 9)$ $\mu m$, as well as with lasers of dissimilar wavelengths.

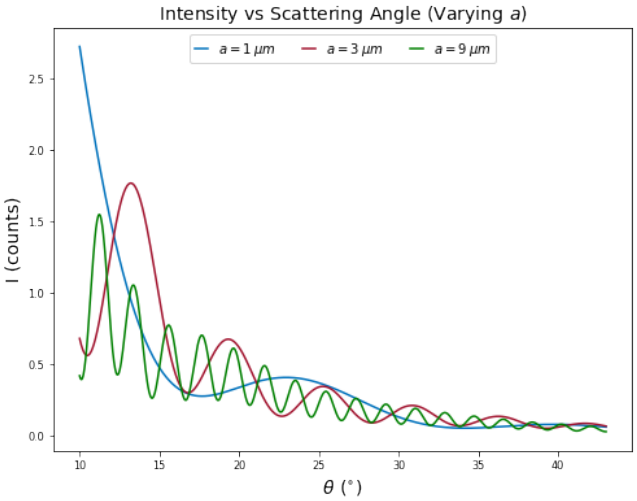


**(a)** Varying sphere diameter.

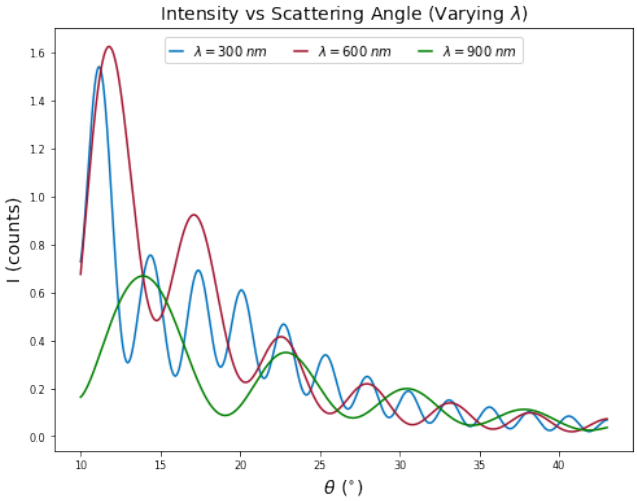


**(b)** Varying laser wavelength.

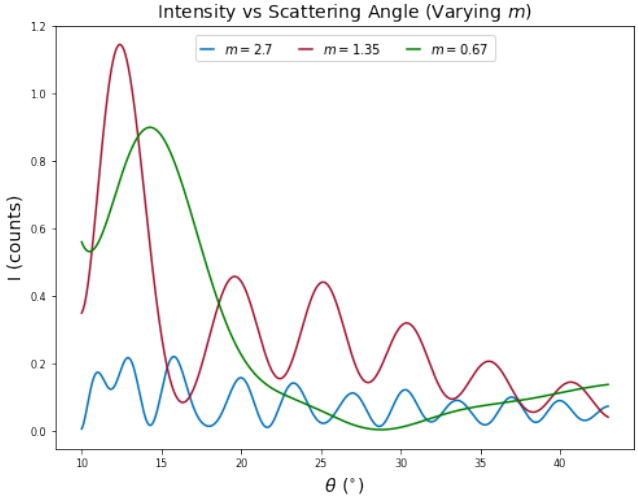


**(c)** Varying the refractive index of the spheres relative to the surrounding medium.

**Fig. 8:** Theoretical angular distributions of scattered intensity produced using MiePython.

## References


[1] W. Hergert and T. Wreidt, *The Mie Theory*, vol. 169, ch. 15-17, pp. 333–4. DOI: 10.1007/978-3-642-28738-1.

[2] R. Drake and J. Gordon, "Mie scattering," *American Journal of Physics*, vol. 53, pp. 955–961, 1985. DOI: 10.1119/1.14011.

[3] I. Weiner, M. Rust, and T. Donnelly, "Particle size determination: An undergraduate lab in mie scattering," *American Journal of Physics*, vol. 69, pp. 129–136, 2001. DOI: 10.1119/1.1311785.

[4] "Miepython." url: https://github.com/scottprahl/miepython /master/miepython/miepython.py.

[5] A. Cox, A. DeWeerd, and J. Linden, "An experiment to measure mie and rayleigh total scattering cross sections," *American Journal of Physics*, vol. 70, pp. 620–625, 2002. DOI: 10.1119/1.1466815.

[6] "Safety data sheet." url: https://www.sigmaaldrich.com/IE/en/sds/ sigma/lb8.

[7] "Safety data sheet." url: https://www.sigmaaldrich.com/IE/en/sds /sigma/89904.


# 6 Appendix

## 6.1 Experimental Corrections

$I_0$ is:

$$I_0 = c\epsilon_0 E_0^2 (m^2 - 1)^2 \frac{a^6 k^4}{18 r^2} \tag{12}$$

with $\epsilon_0$, the permittivity of free space, $m$, the refractive index of the spheres relative to water, $r$, the distance from a sphere, $c$, the speed of light, and $E_0$, the electric field.

$J_1(x)$ is:

$$J_1(x) = \frac{\sin x - x \cos x}{x^2} \tag{13}$$

$x$ is:

$$x = ka\left(1 + m^2 - 2m\cos\theta\right) \tag{14}$$